ACS APPLIED MATERIALS & INTERFACES

Research Article

www.acsami.org

PLLA Microalloys Versus PLLA Nanoalloys: Preparation, Morphologies, and Properties

Wenyong Dong, Fanhui Jiang, Liping Zhao, Jichun You, Xiaojun Cao, and Yongjin Li*

College of Material, Chemistry and Chemical Engineering, Hangzhou Normal University, No. 16 Xuelin Rd., Xiasha High-tech Zone, Hangzhou 310036, People's Republic of China

Supporting Information

ABSTRACT: Nanostructured polymer blends have attracted significant attention recently. In this paper, the poly(lactic acid) (PLLA)/ethylene-co-acrylic ester-co-glycidyl methacrylate (E-AE-GMA) rubber (80/20) nanoalloys and microalloys were fabricated by melt blending and the structure−property relationships of the prepared alloys were investigated. In the nanoalloys, the rubber domains are homogeneously dispersed in the PLLA matrix with the overall domain size of <100 nm. Such nanoalloys exhibit not only high transparency in the visible region, but also significantly improved ductility and impact strength, compared with neat PLLA. Moreover, the nanodomains in the PLLA matrix enhance the crystallization rate of PLLA drastically. The overall crystallization rate of the PLLA nanoalloy is even higher than that of the PLLA nucleated by talc. In contrast, the PLLA microalloy has a phase structure with the size of the rubber domains being in the micrometer to submicrometer scale. The microalloy is opaque and displays almost the same tensile strength and modulus as the nanoalloy, but much higher impact strength than the nanoalloy.

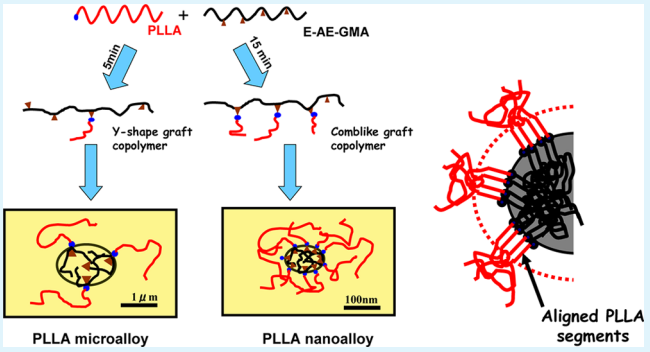

KEYWORDS: *microalloy, nanoalloy, reactive blending, PLLA, crystallization*

1. INTRODUCTION

A growing fraction of all plastic resins produced today are blends of two or more polymers. The blending of polymers with different physical properties presents the possibility of enhancing the overall properties of a material through a synergistic combination of the desirable properties of each component in the system. Almost all polymer pairs are not soluble in each other, because of the high molecular weight, resulting in small mixing entropy contribution; thus, most commercial blends are immiscible.[1] When two immiscible polymers are blended during melt extrusion, a stable morphology is reached in which one phase is mechanically dispersed inside the other. The size and shape of the dispersed phase depends on several processing parameters including rheological and interfacial properties, and the composition of the blend.[2]

Now the phase structure with a micrometer or submicrometer scale, micrometer-structured blends, technically is not difficult to prepare using typical processing methods, such as extrusion or injection molding. The preparation of nanostructured polymer blends from immiscible polymers, with a phase size of <100 nm, has attracted great interest recently. One expects the novel performance (e.g., transparency, heat resistance, creep resistance, etc.) for such nanostructured blends induced by the drastically increased interface/volume ratio and size effects. However, the preparation of nanostructured polymer blends for immiscible polymers is still pretty challenging, using normal processing methods at the present state. Several strategies have been proposed for such purposes.[3−13] Pernot et al. obtained co-continuous nanostructured polyethylene (PE) and PA6 blends by reactive blending. However, this kind of nanostructured co-continuous blend is possible only if the length of all unreacted chains is short enough to be accommodated by the graft copolymer formed in situ.[3,4] Hu el al. has prepared the polypropylene (PP)/PA6 blend with PP dispersed in PA6 several tens of nanometers in size by the in situ polymerization method.[11] One of the authors has succeeded in preparing nanostructured polymer blend using the high shear processing.[12] On the other hand, considerable attention has also been paid to the blending of a homopolymer with a block copolymer containing blocks similar to or miscible with the homopolymer.[13−18] It was shown that the one block of the copolymer can incorporate into the homopolymer and the other blocks form a nanostructured phase that is due to the microphase separation.

Although several strategies have been proposed to fabricate nanostructured polymer blends, the understanding of domain size effects on the properties and physical chemical behaviors of the blends is still not enough, and some contradiction results can be found in previous reports. For example, much literature

Received: April 30, 2012
Accepted: June 19, 2012
Published: June 19, 2012

   dx.doi.org/10.1021/am3007577 | ACS Appl. Mater. Interfaces 2012, 4, 3667−3675

shows that the maximum impact strength was obtained when the rubber particles were in the micrometer to submicrometer scale for rubber-toughened plastic blends.[19−22] However, Pascault et al. insisted that the nanodispersed rubber domains show significant toughening effects for epoxy resin.[16,17] Therefore, it is important to make the detail investigations on the structure and property differences for the nanostructured and microstructured polymer blends, while keeping the blend compositions the same.

On the other hand, poly(lactic acid) (PLLA) has attracted increased attention in recent years. It has been widely used for biomedical applications such as sutures and drug delivery devices as a biodegradable and biocompatible polymer. At the same time, PLLA has also become an alternative to traditional commodity plastics for everyday applications as an environmental friendly polymer, because of its reasonable price and unique properties. Unfortunately, PLLA has a lot of drawbacks, in terms of properties and processability. The inherent brittleness and low heat deflection temperature prevent its use in wide applications. In addition, a high-temperature mold is required for the crystallization of PLLA during melt processing, which results in long processing cycle time and low production efficiency of PLLA products, because of the low crystallization rate. Although numerous investigations have been carried out to modify the properties and processability of PLLA,[23,24] multifunctionality (for example, simultaneously improving the toughness and enhancing the crystallization rate) by a single modifier has not been achieved so far.

In this paper, we have prepared the PLLA alloys by blending with a reactive elastomer containing high concentration epoxide groups. It was found that the microstructured blends (hereafter termed microalloys) and nanostructured PLLA blends (hereafter termed nanoalloys) can be fabricated when using different processing conditions. The comparison has been made for the microalloys and nanoalloys, in terms of the structure and properties, systematically. We found that the nanoalloys and microalloys have almost the same modulus and tensile strength at yielding. However, the nanoalloys show high transparency, excellent ductility, moderate impact strength, and fast overall crystallization rate. In contrast, the microalloy exhibits much higher impact strength than the nanoalloy. To the best of our knowledge, this is the first comparison report on the structure and properties of a nanoalloy and a microalloy with the same compositions by reactive blending. Moreover, we believe that the transparent PLLA nanoalloys prepared in this work open new possibility for the PLLA application as engineering plastics or packaging materials.

2. EXPERIMENTAL SECTION

2.1. Materials and Sample Preparation. The PLLA sample used was bought from Unitika Co. Ltd. (Japan), under the tradename of TP4000. The average molecular weight and molecular weight distribution are reported to be 170 000 and 4.2, respectively. The sample includes 1.2% of D-lactide content. The reactive elastomer is a copolymer of ethylene, acrylic ester, and glycidyl methacrylate (termed as E-AE-GMA) (with the tradename of AX8900) and was purchased from Arkema Co., Ltd. (France). The acrylic ester and glycidyl methacrylate contents in the copolymer are 24 and 8 wt %, respectively. The melt flow rate (MFR) of E-AE-GMA is 6 g/10 min at 190 °C under 2.16 kg. Talc was bought from the Aldrich Chemical Co., Inc., and used as received. The average particle size is ∼2.2 μm.

The PLLA/E-AE-GMA (80/20) blends were prepared using a Laboplasto mill (KF70 V, Toyoseiki Co., Ltd., Japan) with a twin screw at a rotation speed of 100 rpm at 200 °C for various times. After blending, all the samples were hot-pressed at 200 °C to a sheet with a thickness of 500 μm under the pressure of 10 MPa for 5 min, followed by quickly quenching into ice water. The all samples obtained by this process are amorphous, because of the high quenching speed from the melt, which was confirmed by the wide-angle X-ray diffraction (WAXD) measurements, as seen in Figure S1 in the Supporting Information. The PLLA/talc composites with 5 wt % talc were prepared using the same machine at 200 °C for 5 min, and the composite films were made using a hot press and quench process.

2.2. Structural Characterization. Morphology of the blends was observed via field-emission scanning electron microscopy (FE-SEM) and transmission electron microscopy (TEM). A Hitachi Model S4800 SEM system was used for SEM measurements at an accelerating voltage of 10 kV. All the samples were fractured after immersion in liquid nitrogen for ∼10 min. The fracture surface was then coated with a thin layer of gold. TEM analysis was carried out using a Hitachi Model H7000 system at an acceleration voltage of 75 kV. The blend samples were ultramicrotomed at −120 °C to a section with a thickness of ∼70 nm. The sections were then stained with RuO_4 for 20 min.

Dynamic mechanical analysis (DMA) was carried out with a TA Instruments Model Q 800 apparatus in the tensile mode. All the measurements were performed in the linear region with the strain of 0.03%. Dynamic loss (tan δ) was determined at a frequency of 1 Hz and a heating rate of 3 °C/min, as a function of temperature (from −150 °C to 175 °C).

Differential scanning calorimetry (DSC) was carried out under nitrogen flow at a heating rate of 10 K/min with a differential scanning calorimetry (DSC) system (TA Instruments DSC Q1000) calibrated with the melting temperatures of indium and zinc.

Fourier transformed infrared (FTIR) spectra were measured with a VERTEX Model 70v spectrophotometer, using transmission mode. The sample for FTIR measurements was prepared by direct hot-pressing of a melt-blended sample. The thickness is ∼20−40 μm.

The molecular weights and the molecular weight distribution of the prepared alloys were measured at 40 °C using a gel permeation chromatography (GPC) system that was equipped with a Waters 2695 HPLC pump, two columns, and a Waters 2695 refractive index detector. Tetrahydrofuran (THF) was used as a diluent at a flow rate of 1.0 mL/min.

2.3. Physical Property Measurements. Tensile tests were carried out according to the JIS K7113 test method, using dumbbell-shaped samples punched out from the molded sheets. The tests were performed using a tensile testing machine (Instron, Model 5966) at a crosshead speed of 10 mm/min at 20 °C and 50% relative humidity. At least five specimens were tested for each sample. Tensile impact tests were carried out according to JIS K7160 procedures, using a standard impact tester (Toyoseiki Co., Ltd., Japan) at 20 °C and 50% relative humidity. At least five specimens were tested for each sample to get an average value.

3. RESULTS AND DISCUSSION

3.1. Morphologies of PLLA Nanoalloys and Microalloys. Figures 1a and 1b shows SEM images of PLLA/E-AE-GMA 80/20 blends melt-processed for 5 and 15 min, respectively. One should note that the scale bar is different for these two samples. For both samples, the rubber is found to be well-dispersed in the PLLA matrix. However, the morphologies are different. The blend melt-processed for 5 min has a relatively coarse phase morphology with the rubber domain size ranging from 200 nm to 1 μm. The sample is hereafter termed as the microalloy, because of the micrometer to submicrometer dispersion of the rubber domains. On the other hand, all the rubber domains are homogeneously dispersed in the PLLA matrix when the melt-processed time is prolonged to 15 min, with all the other processing parameters being held constant. The domain size of rubber ranges from 10

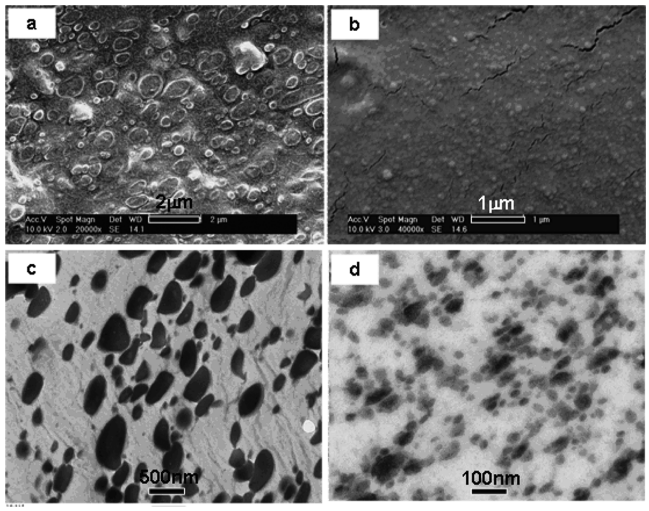

Figure 1. (a) SEM image of PLLA microalloy, (b) SEM image of PLLA nanoalloy, (c) TEM image of PLLA microalloy, and (d) TEM image of PLLA nanoalloy.

nm to 100 nm, which is about one order of magnitude smaller than that in the microalloy. The sample is hereafter termed as the nanoalloy, because the size of the all domains is <100 nm. The phase structures of the blends were further confirmed by TEM, as shown in Figures 1c and 1d. The rubber is observed as a dark phase and PLLA is observed as a bright phase, because the rubber is more easily stained using RuO_4 than the PLLA matrix. It can be seen that the rubber domains are dispersed in the PLLA matrix in the submicrometer scale for the microalloy. However, the size of the rubber phase is much smaller and ranges from 10 nm to 100 nm for the nanoalloy. The domain number-averaged diameters of the microalloys and nanoalloys from TEM images were calculated as follows:

$$D_N = \frac{\sum N_i D_i}{\sum N_i} \quad (1)$$

where D_N is the number-average diameter and N_i is the number of domains with a diameter of D_i. The average domain size of the microalloy is calculated to be 395 nm, and that of the nanoalloy is calculated to be 54 nm. Moreover, the nanoalloys show a much narrower domain size distribution than the microalloys (shown in Figure S2 in the Supporting Information).

3.2. Mechanical Properties. Mechanical properties of the nanoalloy and the microalloy have been evaluated carefully. Note that all the samples (neat PLLA, microalloys, and nanoalloys) used for the property measurements are amorphous, because of the very fast quenching process from the melt state. This is confirmed by WAXD in Figure S1 in the Supporting Information, and no diffraction peaks from PLLA crystals for the all samples were observed. Therefore, the properties are considered to be only dependent on the phase structures of the PLLA alloys. Tensile stress–strain curves of neat PLLA, microalloys, and nanoalloys are shown in Figure 2a. The main tensile properties such as static modulus, tensile stress, and elongation at break, as determined from these curves, are presented in Table 1. PLLA is very rigid and shows pretty high tensile strength, but it breaks at an elongation at break value of ~5%. The incorporation of the soft reactive rubber significantly increases the ductility. Both the microalloy and nanoalloy break at very high strain. The elongation at break

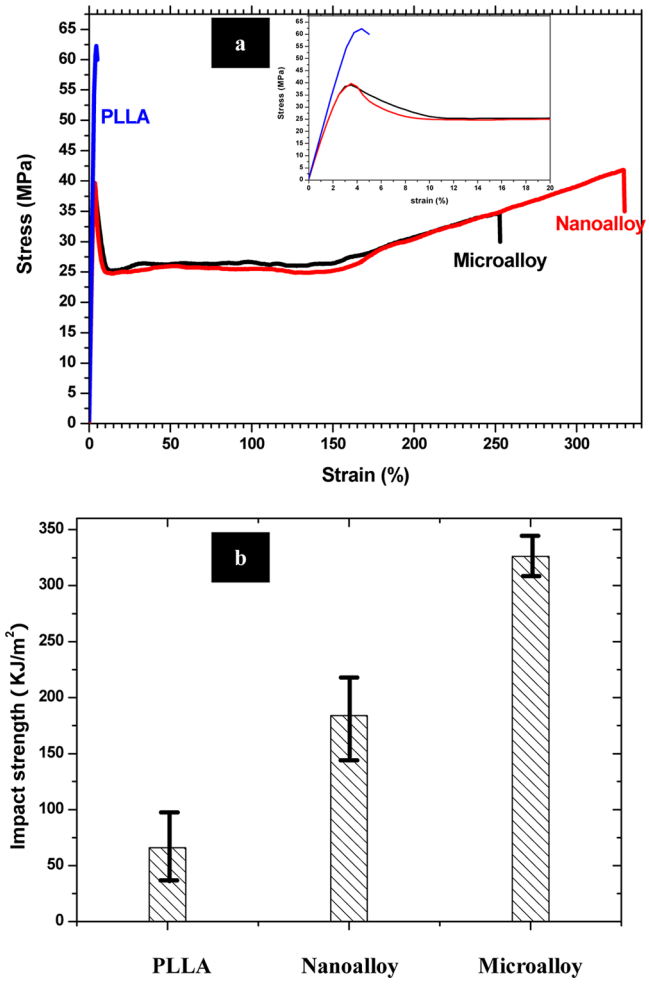

Figure 2. (a) Stress–strain curves and (b) tensile impact strength of neat PLLA, PLLA nanoalloys, and PLLA microalloys.

value of the nanoalloy reaches 329%, which is 66 times higher than that of the neat PLLA. Moreover, one can see that the nanoalloy shows higher elongation at break than the microalloy, indicating better ductility of the nanoalloy.

Although the nanoalloy shows higher ductility than the microalloy, the impact strength of the microalloy is much higher than that of the nanoalloy, as shown in Figure 2b. The impact strengths for neat PLLA, the nanoalloy, and the microalloy are 69.5, 183, and 331 kJ/m^2. To improve toughness, effective toughening mechanisms must be generated. Massive crazing and shear yielding are the two most frequently encountered energy-absorbing mechanisms.[25−27] Criteria for the occurrence of crazing and shear yielding are widely discussed and well understood.[25,27−29] We have compared the toughening mechanism of the nanoalloy and the microalloy using double-notched impact method, as shown in Figure 3a. From TEM investigation, it is seen that a large amount of rubber particles are cavitated in the damage zone of the microalloys (Figure 3b). In comparison, no particle cavitation is found in the domains in the nanoalloys, but the nanodomains are elongated along the impact direction after the impact tests (Figure 3c). This observation indicates that that only the large rubber particles in submicrometer scale are effective in triggering crazes to dissipate impact energy, which is consistent with many previous results.[25−27] The nanodomains in the nanoalloy cannot cavitate effectively and only massive

Table 1. Mechanical Properties of PLLA/E-AE-GMA Blends

sample	tensile modulus (GPa)	tensile strength at yielding (MPa)	tensile strength at break (MPa)	elongation at break (%)	impact strength (kJ/m^2)
PLLA	2.81 ± 0.04		65.5 ± 4.2	4.1 ± 2	69.5 ± 27
PLLA microalloy	1.02 ± 0.03	40.2 ± 0.8	34.6 ± 3.3	252 ± 21	331 ± 16
PLLA nanoalloy	1.05 ± 0.03	40.2 ± 1.0	41.8 ± 2.2	329 ± 17	183 ± 32

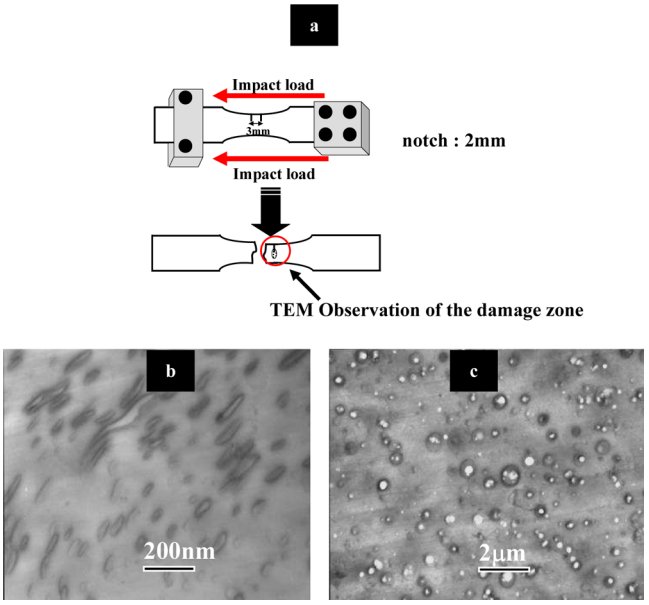

Figure 3. (a) Schematic diagram of the double-notch impact test; (b) TEM image of damage zone in the PLLA nanoalloys; and (c) TEM image of damage zone in the PLLA microalloys.

deformation in the nanodomains can be observed after the impact tests, so the impact strength of the nanoalloys is lower than that of the microalloy. Note that the plastic deformation induced by rubber nanodomains can also absorb impact energy upon the impact test, so the impact strength of the nanoalloys is higher than that of neat PLLA.

It is well-known that the matrix ligament thickness (defined as the surface-to-surface dispersed-phase interparticle distance) is an important parameter to evaluate the toughness of a rubber-toughened plastic blend. Wu suggested that the brittle–ductile transition can only be observed when the matrix ligament thickness is below the critical value.[30,31] The calculated matrix ligament thickness values for the nanoalloy and the microalloy are 121 and 554 nm, respectively, according to the calculation method by Choy.[32] Anderson et al. reported that the critical matrix ligament thickness of PLLA was ca. 1.0 μm.[33] Such critical value is higher than the ligament thickness for both the nanoalloy and the microalloy. Therefore, the significant increased impact strength for both nanoalloys and microalloys were achieved, compared with neat PLLA.

3.3. Optical Properties of the PLLA Nanoalloys and Microalloys. Optically transparent heterogeneous polymeric materials have attracted significant attention, because they combine the excellent physical properties of different phases in addition to exhibiting optical clearance. According to the Rayleigh Scattering Law, the scattering loss in a heterogeneous system is dependent on the relative size of the dispersed phase to the wavelength and also the difference in the refractive index of the two phases.[34] Therefore, the size of the dispersed phase is critically important in reducing the scattering loss if the refractive indexes are different for the two components.

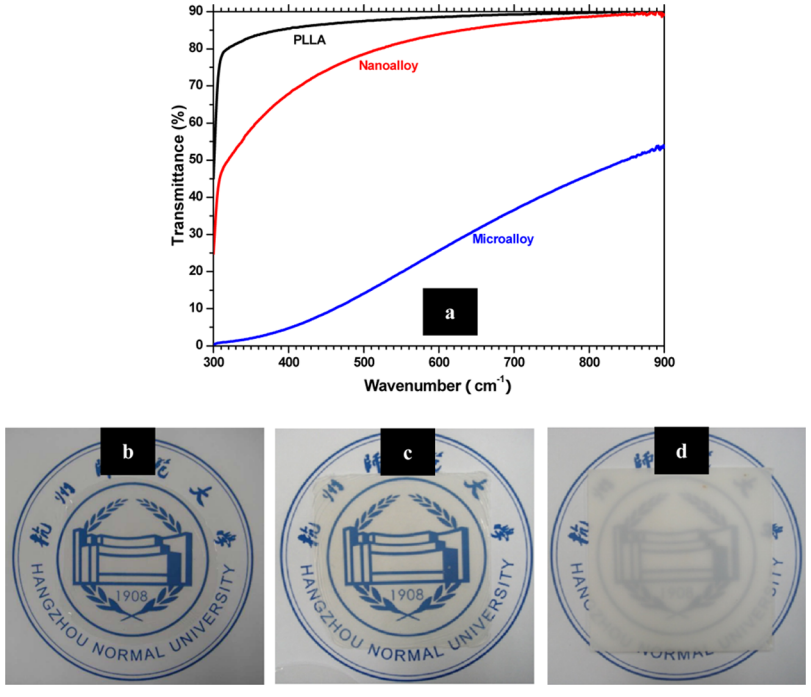

Figure 4. (a) UV-vis transmittance spectra of pure PLLA (black trace), PLLA nanoalloy (red trace), and PLLA microalloy (blue trace). Also shown are photographs of (b) the neat PLLA, (c) the PLLA nanoalloy, and (d) the PLLA microalloy (the thickness of the sheets is ~200 μm).

Generally, one must achieve a homogeneous dispersion of domains <100 nm in size to obtain a transparent heterogeneous material. The PLLA nanoalloy fulfills such a requirement, as shown in Figure 4. Figure 4a shows the quantitative ultraviolet−visible light (UV-vis) transmittance spectra of the neat PLLA, PLLA nanoalloy, and PLLA microalloy. All samples have a thickness of ∼200 μm. Neat PLLA exhibits a very high transmittance of ∼88% above a wavelength of 450 nm. The nanoalloys exhibit a slightly decreased transmittance over the entire spectrum region, compared with the neat PLLA. The transmittance in the visible region is above 80% in the visible region, indicating the high clearance of the prepared nanoalloy. In contrast, the microalloys show much lower transmittance, when compared with the nanoalloy and the neat PLLA, over the entire wavelength region. Figure 4 shows also photographs of the hot-pressed film obtained from the correspondence samples. It is clear that the nanoalloy exhibits excellent optical transparency, while the microalloy sample is opaque. Obviously, the difference in transparency between the nanoalloy and the microalloy originates only from the domain size effects, because both the nanoalloy and the microalloy are amorphous. The transparent PLLA nanoalloy might be used as packaging material when the clearance properties are required.

3.4. Dynamic Mechanical Analysis. Figure 5 demonstrates the storage modulus and dynamic loss curves as a function of temperature for the neat PLLA, the neat elastomer, the microalloy, and the nanoalloy. All of the PLLA samples used for the measurements are amorphous. Neat PLLA has a higher modulus (E') than both the microalloy and the nanoalloy in the temperature region of <60 °C. The E' value of neat PLLA and its alloys dropped abruptly at ∼50−60 °C, because of the glass transition of PLLA, and then rose at temperatures ranging from 80 °C to 140 °C, because of the cold crystallization of PLLA.[35] The temperature at which E' starts to increase, because of the crystallization of the PLLA component for nanoalloys, is lower than that of neat PLLA and microalloys. This result suggests that the nanodomains in the nanoalloys enhance the cold crystallization ability of PLLA and, therefore, the cold crystallization of PLLA in the nanoalloys starts at lower temperature.

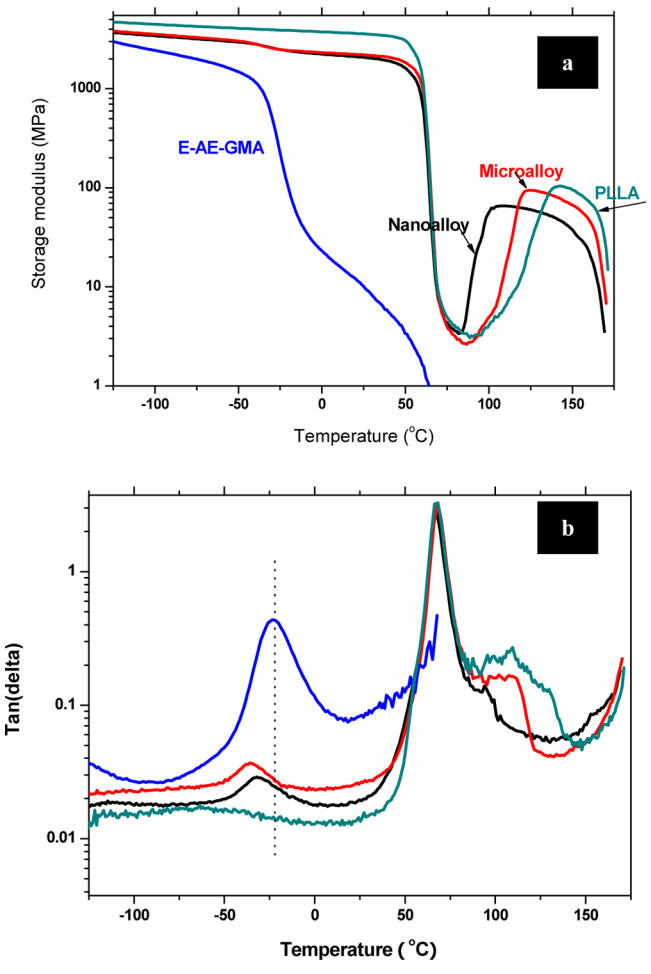

Figure 5. Temperature dependence of (a) the dynamic storage modulus and (b) the dynamic loss (tan δ) for the indicated samples.

From the figure with the dynamic loss curves (Figure 5b), it is observed that the glass-transition temperature (T_g) values for PLLA in both the microalloy and the nanoalloy are the same as that of the neat PLLA, indicating that reactive blending does not change the T_g values for PLLA. However, the T_g value corresponding to the elastomer decreases drastically after blending with PLLA. The T_g value of the neat elastomer is −23.7 °C. However, the T_g value corresponding to the elastomer phase for the nanoalloy is −31.3 °C, and that for the microalloy is −35.1 °C. The depression of the T_g value in the rubber phase has been observed previously.[36−40] It is generally accepted that the T_g depression in the rubber phase originates from the asymmetric thermal shrinkage in the rubber phase and the matrix plastic phase.[36−40] It is interesting to find the domain size dependence of the T_g depression in the rubber phase. The high density of grafted copolymers at the interface between the PLLA matrix and the rubber domains for nanoalloys impede the asymmetric thermal shrinkage, so a smaller T_g depression was observed for the nanoalloys, compared to that observed for the microalloys. The details regarding the mechanism of this phenomena and the relationship of the T_g depression with the impact strength are under investigation.

3.5. Crystallization Behaviors of PLLA Nanoalloys and Microalloys. PLLA crystallizes very slowly from both the melt state and the glassy state, which leads to the need for high mold temperature and long processing cycle time to make the fully crystalline PLLA products. Our investigation shows that the PLLA nanoalloys crystallize very quickly and the nanodomains represent a highly efficient nucleation agent for the PLLA matrix. Figure 6a shows the DSC cooling curves (the cooling rate is 10 °C/min) of the neat PLLA, the PLLA nanoalloy, the PLLA microalloy, and the PLLA nucleated by 5 wt % talc. All of the samples suffered the same thermal history, which consisted of first heating the samples to 220 °C and then keeping them at that temperature for 5 min. No crystallization peaks were observed for the neat PLLA and the PLLA microalloy, indicating that the PLLA does not crystallize at a cooling rate of 10 °C/min. However, the PLLA nanoalloy shows a sharp and symmetric exothermal crystallization peak, which means that PLLA in the nanoalloy can be crystallized under the given cooling conditions. Talc has been reported to be one of the best nucleation agents for PLLA. For comparison, the PLLA/talc composites with 5 wt % talc have been prepared. For the present composites, talc is well-dispersed in the PLLA matrix, as shown in Figure S3 in the Supporting Information. Therefore, it is expected that the talc acts as an effective nucleation agent for PLLA. The DSC cooling curve for this composite is also shown in Figure 6a. The talc-nucleated PLLA

dx.doi.org/10.1021/am3007577 | ACS Appl. Mater. Interfaces 2012, 4, 3667−3675

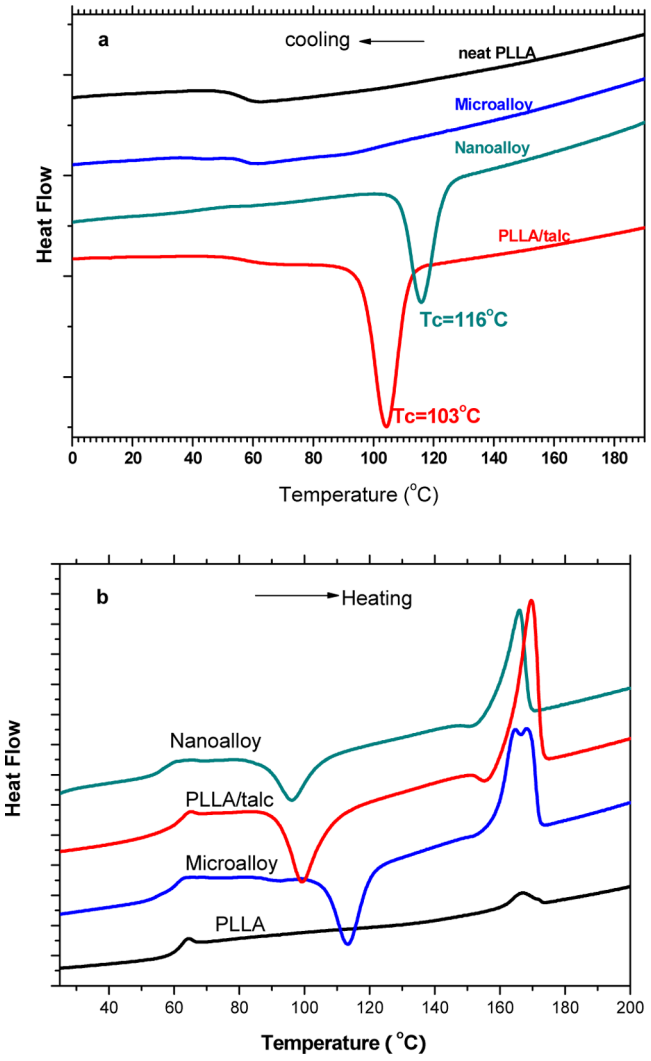

Figure 6. (a) DSC cooling curves (10 °C/min) from 220 °C after being held at that temperature for 5 min, and (b) DSC heating curves (10 °C/min) for the quenched samples from room temperature.

can also crystallize at a cooling rate of 10 °C/min from the melt state. However, the crystallization onset temperature and the crystallization peak temperature for the nanoalloy are 125 and 116 °C, respectively, compared to 111 and 103 °C for the talc-nucleated PLLA. The much-higher crystallization temperature of the nanoalloy means that the crystallization rate of the nanoalloy is higher than that of the talc-nucleated PLLA. Such results indicate that the nanodomains in the PLLA nanoalloy are efficient nucleation sites for the PLLA matrix and the nucleation effects are greater than those for the widely used talc. Observation via optical microscopy shows that the crystal size in the nanoalloys is much smaller than that in the neat PLLA (see Figure S4 in the Supporting Information). Moreover, the heat of the melt crystallization of the nanoalloy based on the PLLA weight percentage and that of the talc-nucleated PLLA are 36 J/g and 29.5 J/g, respectively, indicating that a higher fraction of amorphous PLLA crystallizes in the nanoalloys than in the PLLA/talc composites, when cooling from the melt at the same cooling rate. The thermal properties for the all samples are shown in Table 2.

The nucleation effects of the nanodomains in the nanoalloy can also be observed for the cold crystallization when heating

Table 2. Thermal Properties of Neat PLLA, the Nanoalloy, the Microalloy, and the Reactive Rubber

	T_g (°C)						
sample	rubber	PLLA	T_{mc}[a] (°C)	T_{cc}[b] (°C)	ΔH_{cc} (J/g)	ΔH_{mc} (J/g)	χ[c] (%)
neat PLLA		67.5			4.8	0	0
nanoalloy	−31.3	67.4	116	96.1	41.2	36.0	38.7
microalloy	−35.1	67.5		113	43.2	0	0
PLLA/Talc		67.8	103	99.5	41.8	29.5	31.7
E-AE-GMA	−23.7						

[a]Peak temperature during melt crystallization. [b]Peak temperature during cold crystallization. [c]The calculated crystallinity for the melt crystallization simply calculated by the ratio of the enthalpies of the melt crystallization to 93 J/g, which was reported to be the melting enthalpy for 100% crystallized PLLA.

the quenched amorphous nanoalloys from low temperature. Figure 6b shows the DSC heating curves from room temperature at a heating rate of 10 °C/min for the neat PLLA, nanoalloy, and microalloy. The cold crystallization peak temperature and the crystallization exotherm entropy are also tabulated in Table 2. The cold crystallization peak temperature of the nanoalloy is 17.5 °C lower than that of the microalloy, again indicating the significant nucleation effects of the nanodomains for the crystallization of PLLA in the nanoalloys. Note that the cold crystallization peak temperature of the microalloy is lower than that of neat PLLA, which suggests that the crystallization rate of PLLA in the microalloy is higher than that of neat PLLA.

4. DISCUSSION

We have found that simply prolonging the melting mixing time for PLLA with the commercially available reactive polyolefin elastomer results in a nanoalloy with excellent mechanical properties, high transparency, and enhanced crystallization rate. The reaction between the end −COOH groups of PLLA and epoxide groups has been reported previously.[40−44] In the present investigation, the reaction occurs gradually with increasing mixing time, as shown the continuously increased the mixing torque with the time in Figure 7. The torque for the neat PLLA decreases gradually due to the hydrolysis during

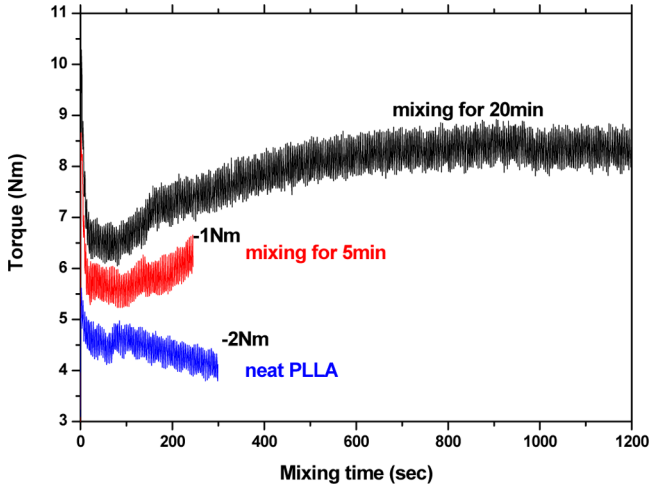

Figure 7. Mixing torque as a function of the mixing time for neat PLLA and PLLA/E-AE-GMA blends.

melt mixing. However, the melt mixing of PLLA with the reactive rubber induces continuously increased torque after the initial decreasing by the melt of solid pellets, indicating the reaction between PLLA with E-AE-GMA. It is seen that the torque levels off after 15 min mixing, suggesting the end of the reaction. At the same time, the FTIR investigation presents the direct evidence for the reaction between epoxide groups in rubber and end groups in PLLA, as shown in Figure 8. Trace of

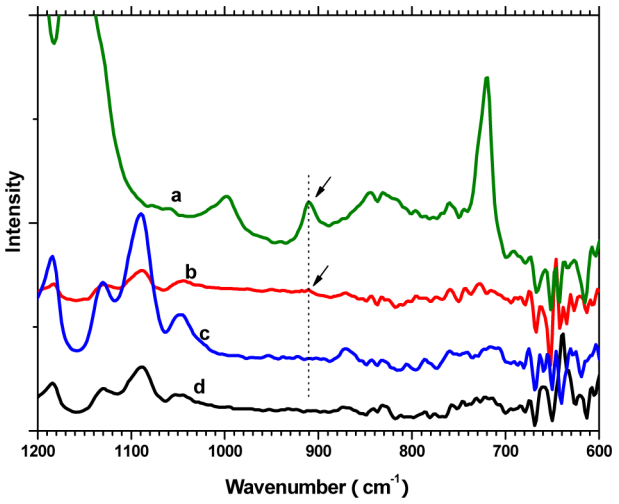

Figure 8. FTIR spectra for the (a) E-AE-GMA rubber, (b) PLLA microalloy, (c) PLLA nanoalloy, and (d) neat PLLA.

epoxide absorption at 910 cm^{-1} was observed for the microalloys, but the peak disappeared for the nanoalloys. Therefore, morphology development during the reactive blending of PLLA with E-EA-GMA may be schematically summarized in Figure 9. In the early stage, few PLLA molecules react with the epoxide groups in the rubber chains to form the Y-shaped graft copolymer. Such graft copolymer works as the compatibilizer and locates at the interface between PLLA and the reactive rubber phase. The rubber forms a dispersed phase in the PLLA matrix and the domain size ranges from micrometer scale to submicrometer scale. The micrometer-sized rubber domains can be easily cavitated upon the impact tests and absorb massive impact energy. By prolonging the melt mixing time, significantly enhanced grafting reaction occurs at the interface, thus creating a large amount of comblike graft copolymer. In the melt, the resulting comblike graft copolymers self-assemble into nanostructured micelles with the rubber chains as the nanodomains are dispersed in the PLLA matrix and the nanoalloys were obtained.

In the nanoalloys, the nanodomains not only enhance the ductility and the impact strength of the materials, but also accelerate the overall crystallization rate of PLLA significantly. Such nucleation agent effects are very important for PLLA-based materials, because they will shorten the processing cycle time and increase crystallinity to improve the heat resistance of the materials. In fact, the enhancement effect of nucleation and crystallization in immiscible blends has been documented in several papers. Bartczak et al.[45] and Wenig et al.[46] suggested that the enhanced crystallization in immiscible blends is caused by a decrease in the surface free energy of formation of crystal nuclei, because of the presence of the phase interface. Han et al. investigated the relationship between nucleation and liquid–liquid phase separation (LLPS) in the poly(ethylene-co-

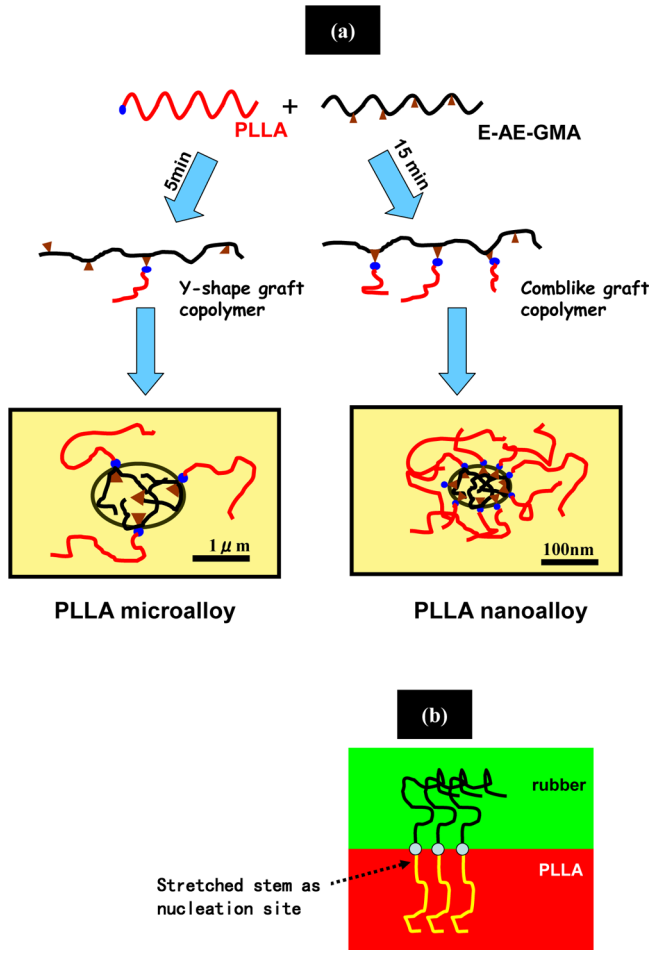

Figure 9. (a) Schematic diagrams of morphology development of PLLA/E-AE-GMA blend during the reactive blending, and (b) schematic diagram at the interface between the PLLA matrix and the rubber domains for nanoalloys.

butene)/poly(ethylene-co-hexene) (PEB/PEH) blend system and claimed that the nuclei mainly resided near the interface of the phases, because of a specific orientation of polymer chains.[47−49] Recently, Yazawa et al. revealed that the depressed T_g value locally at the interface of PCL domains accelerate the nucleation of the PLLA in the PLLA/PCL blends.[50] However, all these systems are the physical melt blending without the chemical reactive and no crystallization dependence on domain size was reported. In the present case, we found that the enhancement of the crystallization rate is highly dependent on the rubber domains size and the nanodomains are more effective than the microdomains. Obviously, the formed graft copolymers are the strongly segregated system because PLLA is immiscible with E-AE-GMA. In the nanoalloys, the grafted PLLA chains are densely located at the interfaces. The strongly segregated comblike graft copolymer could have induced PLLA segmental alignment and orientation (relative to chain in bulk) at the interface, as schematically illustrated in Figure 9b. These aligned PLLA segments may attach themselves to become nuclei or the precursor of nuclei for crystallization during cooling from the melt state. In the nanoalloys, high concentration of such aligned PLLA chains induces the enhanced nucleation rate, followed by the crystal growth of PLLA in the matrix from the nuclei.

One should pay attention to the possible degradation of PLLA during the melt mixing. PLLA is easily degraded during the melt processing, because of the hydrolysis of the aliphatic polyester, as also shown by the decreasing torque in Figure 7. We have evaluated the molecular weight of the nanoalloy and the microalloy, using GPC measurements, and the results are shown in Figure 10. An obvious decrease in manganese content

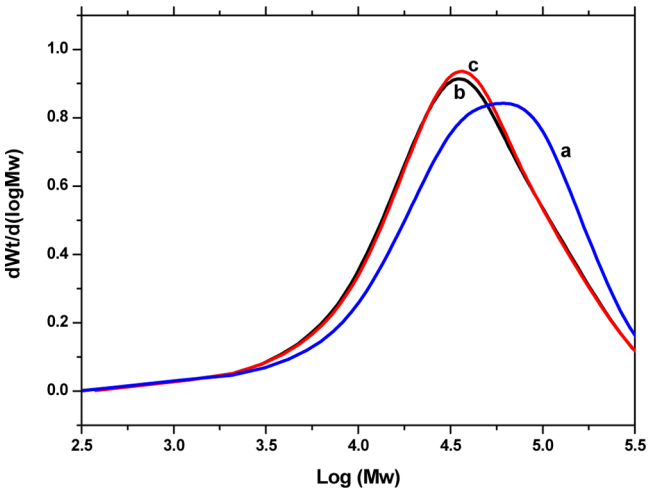

Figure 10. GPC curves of (a) neat PLLA before melt mixing, (b) the nanoalloy, and (c) the microalloys.

was observed for the microalloy, compared with the PLLA before mixing. However, one can find that the molecular weight of the nanoalloy with the 15 min melt processing is almost same as that of the microalloy by short time mixing. It is considered that the chemical grafting of the reactive rubber on the PLLA chain during melt mixing may balance the chain hydrolysis of PLLA at high temperature.

5. CONCLUSIONS

We have achieved a homogeneous dispersion of rubber domains <100 nm in size in a PLLA matrix to obtain PLLA nanoalloys. The nanoalloys combine the excellent ductility and improved impact strength in addition to high optical clearance. Moreover, the aligned PLLA segments near the interface by the reactive blending in the nanoallys nucleate easily, because of the decreased entropy, which results in the significantly enhanced nucleation rate. On the other hand, the lesser reaction using short mixing time leads to a microalloy with the rubber domains size in micrometer and submicrometer scale. The rubber domains in the micrometer scale can be cavitated effectively and dissipate massive impact energy, so the microalloys exhibit the much higher impact strength than the nanoalloys and neat PLLA.

■ ASSOCIATED CONTENT

Supporting Information

WAXD, domain size distribution, SEM for PLLA/talc, and POM images of nanoalloy and microalloy. This information is available free of charge via the Internet at http://pubs.acs.org.

■ AUTHOR INFORMATION

Corresponding Author

*Tel.: +86-571-28866579. Fax: +86-571-28867899. E-mail: yongjin-li@hznu.edu.cn.

Notes

The authors declare no competing financial interest.

■ ACKNOWLEDGMENTS

This work was financially supported by the National Natural Science Foundation of China (Nos. 51173036, 21074029, 21104014, 21104013) and Zhejiang Provincial Natural Science Foundation of China (No. R4110021). This work was also partially supported by the Project of Zhejiang Key Scientific and Technological Innovation Team (No. 2010R50017).

■ REFERENCES

(1) Utracki, L. A. *Polymer Blends Handbook*; Kluwer Academic Publishers: Dordrecht, The Netherlands, Boston, 2003.
(2) Uttandaraman, S.; Macosko, C. W. *Macromolecules* **1995**, *28*, 2647.
(3) Pernot, H.; Baumert, M.; Court, F.; Leibler, L. *Nat. Mater.* **2002**, *1*, 54.
(4) Gani, L.; Tencé-Girault, S.; Millequant, M.; Bizet, S.; Leibler, L. *Macromol. Chem. Phys.* **2010**, *211*, 736−743.
(5) Wildes, G. S.; Harada, T.; Keskkula, H. *Polymer* **1999**, *40*, 3069.
(6) Frisch, H. L.; Frisch, K. L.; Klempner, D. *Polym. Eng. Sci.* **1974**, *14*, 646.
(7) Robeson, L. M.; Furtek, A. B. *J. Appl. Polym. Sci.* **1979**, *23*, 645.
(8) Paul, D. R. *Macromol. Symp.* **1994**, *78*, 83.
(9) Charoensirisomboon, P.; Inoue, T.; Weber, M. *Polymer* **2000**, *41*, 4483.
(10) Ibuki, J.; Charoensirisomboon, P.; Chiba, T.; Ougizawa, T.; Inoue, T.; Weber, M.; Koch, E. *Polymer* **1999**, *40*, 647.
(11) Hu, G. H.; Cartuer, H.; Plummer, C. *Macromolecules* **1999**, *32*, 4713.
(12) Li, Y.; Shimizu, H. *Polym. Eng. Sci.* **2011**, *51*, 1437.
(13) Corte, L.; Leibler, L. *Macromolecules* **2006**, *39*, 2445.
(14) Koulic, C.; Jerome, R. *Macromolecules* **2004**, *37*, 888.
(15) Koulic, C.; Jerome, R. *Macromolecules* **2004**, *37*, 3459.
(16) Ritzenthaler, S.; Court, F.; David, L.; Girard-Reydet, E.; Leibler, L.; Pascault, J. P. *Macromolecules* **2002**, *35*, 6245.
(17) Ritzenthaler, S.; Court, F.; Girard-Reydet, E.; Leibler, L.; Pascault, J. P. *Macromolecules* **2003**, *36*, 118.
(18) Jouenne, S.; Gonzalez-leon, J. A.; Ruzette, A.; Lodefier, P.; Leibler, L. *Macromolecules* **2008**, *41*, 9823.
(19) Wu, S. *Polym. Eng. Sci.* **1987**, *27*, 335.
(20) Jancar, J.; Di Anselmo, A.; Di Benedetto, A. T.; Kucera, J. *Polymer* **1993**, *34*, 1684.
(21) D'Orazio, L.; Mancarela, C.; Martuscelli, E.; Sticotti, G.; Massari, P. *Polymer* **1993**, *34*, 3671.
(22) Chou, C. J.; Vijayan, K.; Kirby, D.; Hiltner, A.; Baer, E. *J. Mater. Sci.* **1988**, *23*, 2521.
(23) Anderson, K. S.; Hillmyer, M. A. *Polymer* **2006**, *47*, 2030.
(24) Liu, H.; Zhang, J. *J. Polym. Sci. Polym. Phys.* **2011**, *49*, 1051.
(25) Donald, A. M.; Kramer, E. J. *J. Appl. Polym. Sci.* **1982**, *27*, 3729.
(26) Kinlock, A. J.; Young, R. J. *Fracture Behavior of Polymers*; Applied Science: London, 1983.
(27) Sue, H. J.; Yee, A. F. *J. Mater. Sci.* **1989**, *24*, 1447.
(28) Yee, A. F.; Pearson, R. A. *J. Mater. Sci.* **1986**, *21*, 2462.
(29) Yee, A. F.; Pearson, R. A. *J. Mater. Sci.* **1986**, *21*, 2475.
(30) Wu, S. *Polymer* **1985**, *26*, 1855.
(31) Wu, S. *J. Appl. Polym. Sci.* **1988**, *35*, 549.
(32) Liu, Z. H.; Zhang, X. D.; Zhu, X. G.; Li, R.; Qi, Z. N.; Wang, F. S.; Choy, C. L. *Polymer* **1998**, *39*, 5019.
(33) Anderson, K. S.; Lim, S. H.; Hillmyer, M. A. *J. Appl. Polym. Sci.* **2002**, *89*, 2331.
(34) Bohren, F. B.; Huffman, D. R. *Absorption and Scattering of Light by Small Particles*; John Wiley & Sons, Inc.: New York, 1983.
(35) Li, Y. J.; Shimizu, H. *Macromol. Biosci.* **2007**, *7*, 921.
(36) Pavan, A.; Riccó, T. *J. Mater. Sci.* **1976**, *11*, 1180.
(37) Bates, F. S.; Cohen, R. E.; Argon, A. S. *Macromolecules* **1983**, *16*, 1108.

(38) Argon, A. S.; Cohen, R. E.; Gebizlioglu, O. S.; Schwier, C. E. *Adv. Polym. Sci.* **1983**, *52/53*, 276.
(39) Inoue, T.; Ogata, S.; Kakimoto, M.; Imai, Y. *Macromolecules* **1984**, *17*, 1417.
(40) Su, Z. Z.; Li, Q.; Liu, Y.; Hu, G.; Wu, C. *Eur. Polym. J.* **2009**, *45*, 2428.
(41) Oyama, H. *Polymer* **2009**, *50*, 747.
(42) Liu, H.; Song, W.; Chen, F.; Guo, L.; Zhang, J. *Macromolecules* **2011**, *44*, 1513.
(43) Liu, H.; Chen, F.; Liu, B.; Estep, G.; Zhang, J. *Macromolecules* **2010**, *43*, 6058.
(44) Anderson, K. S.; Schreck, K. M.; Hillmyer, M. A. *Polym. Rev.* **2008**, *48*, 85.
(45) Bartczak, Z.; Galeski, A.; Krasnikova, N. P. *Polymer* **1987**, *28*, 1627.
(46) Wenig, W.; Asresahegn, M. *Polym. Eng. Sci.* **1993**, *33*, 877.
(47) Zhang, X.-H.; Wang, Z.-G.; Dong, X.; Wang, D.-J.; Han, C. C. *J. Chem. Phys.* **2006**, *125*, 024907.
(48) Zhang, X.-H.; Wang, Z.-G.; Muthukumar, M.; Han, C. C. *Macromol. Rapid Commun.* **2005**, *26*, 1285.
(49) Wang, H.; Shimizu, K.; Hobbie, E. K.; Wang, Z.; Meredith, J. C.; Karim, A.; Amis, E. J.; Hsiao, B. S.; Hsieh, E. T.; Han, C. C. *Macromolecules* **2002**, *35*, 1072.
(50) Sakai, F.; Nishikawa, K.; Inoue, Y.; Yazawa, K. *Macromolecules* **2009**, *42*, 8335.